Performance of Eddy Viscosity Model in Rotating Channel Flow

Krishnan V. Pagalthivarthi and **Pankaj K. Gupta**

Dept. of Applied Mechanics, Indian Institute of Technology, Hauz Khas, New Delhi 110016

Abstract: Traditionally, rotation-modified higher order turbulence models are used in simulation of flow through rotating channel. In modeling two-phase flow, prediction of the corresponding single-phase flow is usually an important part of the overall iteration process. Thus, every effort is made to reduce computation time during this part of the solution. With this view, this study employs a rotation-modified eddy viscosity to predict developing mean flow in a rotating channel. Furthermore, in contradistinction with the usually employed parabolic or partially parabolic methods, this study employs an elliptic method. Galerkin finite element method with bilinear velocity interpolation and constant pressure is used. Combined quasi-Newton's iteration enables the simultaneous solution for velocity and pressure fields. The effect of wall functions (with and without modification for rotation) on the friction velocity is presented. Results with modification for rotation compare favorably with experiments, while those with standard wall functions do not.

Key words: *Developing Flow, Galerkin Finite Element Method, Combined quasi-Newton iteration, Rotation-Modified Wall Function and Eddy Viscosity*

INTRODUCTION

In a rotating channel, the Coriolis force has three effects: (1) development of a cross-stream pressure gradient, (2) occurrence of a secondary mean motion, and (3) modification of the turbulent mixing process. Even for a relatively small rotation number ($Ro_H = \Omega U_0 / H$, where Ω is the angular velocity of the channel, U_0 is the inlet mean velocity, and H is the height of the channel), the Coriolis force induces instability (stability) on the pressure (suction) side boundary layer [1]. The differential experience of rotation on the two sides of the channel modifies the turbulent mixing process and causes stabilization (or destabilization) of flow.

Numerical prediction methods [2-5] have primarily relied on parabolic or partially parabolic procedures due to the relatively higher computational cost of elliptic methods. Due to the possibility of secondary flow, the numerical method (whether parabolic or elliptic) must, in general, take the three-dimensionality of the flow into consideration. In addition, it turns out that the standard k- or mixing length models have to be modified [3, 6] to account for rotation effects on turbulence in order to reliably predict the observed asymmetry. Richardson number [1] is a useful parameter in developing such Coriolis-modified turbulence models for rotating flows. Nonlinear Reynolds stress-mean strain rate relationship significantly improves secondary flow prediction for low-aspect ratio ducts [4].

For ducts with an aspect ratio of 7:1 or larger, practically no secondary flow occurs [7]. In such cases, the flow may be treated as essentially two-dimensional. Thus, fully developed flow in rotating channel has been studied [8] to test the performance of second-moment closure models. The cost effectiveness of a two-dimensional model is particularly attractive when dealing with computation-intensive simulations of two-phase flow through rotating channels. In two-phase flow problems, the corresponding single-phase flow solution is an important part of the overall iteration process [9]. In a recent study, two-dimensional (elliptic) prediction of inviscid free surface flow in a rotating channel [10] was reported. This method was extended to viscous free surface flow prediction in a rotating channel [11].

An important extension of [8] is the prediction of two-dimensional *developing* flow in a large-aspect ratio duct. This less-attended problem is the subject of this study. Generally, finite volume or finite difference methods are used for rotating flow problems. This study departs from this trend by employing a Galerkin finite element method. The Reynolds-averaged Navier Stokes equations governing two-dimensional developing flow in a rotating channel (with a large aspect ratio) are cast into weak form using Galerkin finite element method with primitive variables. A rotation-modified eddy viscosity model is used, keeping in mind the extension of this study to two-phase flow. Wall functions with and without modification for rotation are used to compute the friction velocity, which appears in the expression for eddy viscosity.

MATHEMATICAL FORMULATION

In Figure 1, a channel rotating about the z-axis is shown with uniform inflow. The continuity and momentum equations governing steady, incompressible flow in a rotating frame of reference are presented in [12]. From these, the Reynolds-averaged equations in a rotating reference frame may be obtained following the standard procedure [13]. The Boussinesq approximation governing mean rate of strain and Reynolds stress is used to introduce an eddy viscosity into the equations.

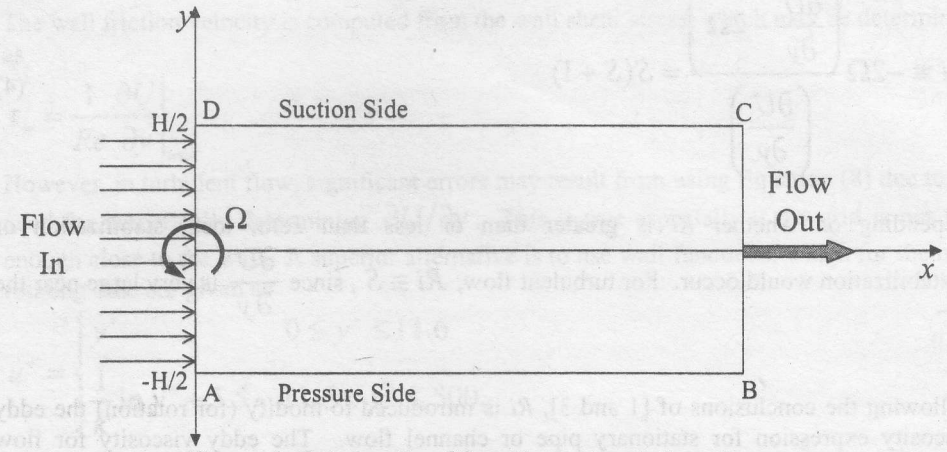

Figure 1. Schematic of flow through rotating channel.

The final governing equations are programmed in non-dimensional form. Mean velocity components U and V (in the x and y directions, respectively) are non-dimensionalized with respect to the uniform inlet mean velocity, U_0; mean pressure, P, with respect to ρU_0^2 (ρ being the density); Ω (angular velocity) with respect to U_0/L; and all lengths with respect to channel length L. Thus in non-dimensional form, the governing equations are

$$\frac{\partial U}{\partial x}+\frac{\partial V}{\partial y}=0, \tag{1}$$

$$U\frac{\partial U}{\partial x}+V\frac{\partial U}{\partial y}=\Omega^2 x+2\Omega V+\frac{\partial}{\partial x}\left(\frac{2\alpha}{Re}\frac{\partial U}{\partial x}-P\right)+\frac{\partial}{\partial y}\frac{\alpha}{Re}\left(\frac{\partial U}{\partial y}+\frac{\partial V}{\partial x}\right), \tag{2}$$

and

$$U\frac{\partial V}{\partial x}+V\frac{\partial V}{\partial y}=\Omega^2 y-2\Omega U+\frac{\partial}{\partial x}\frac{\alpha}{Re}\left(\frac{\partial U}{\partial y}+\frac{\partial V}{\partial x}\right)+\frac{\partial}{\partial x}\left(\frac{2\alpha}{Re}\frac{\partial V}{\partial y}-P\right), \tag{3}$$

where $Re=\dfrac{\rho U_0 L}{\mu}$ is the bulk flow Reynolds number, and α is the ratio of total viscosity (turbulent + laminar) to the laminar viscosity.

The eddy viscosity for a rotating flow must be specified carefully. The Coriolis body force in a rotating channel is analogous to the centrifugal forces associated with curved streamlines and buoyancy forces in density-stratified flows. Based on this similarity, a gradient Richardson number is defined [14] as

The computational exit is located a little distance, ΔL, downstream of the actual channel exit ($x = 1$). Thus, zero-gradient boundary conditions may be applied at the computational exit without introducing significant error. For turbulent flow simulation, along $y = \pm\frac{H}{2}$, wall functions, as shown in Equation (11), may also be used.

NUMERICAL METHOD

Galerkin formulation [17] is used to transform the governing equations into algebraic form. The velocity components, *U* and *V*, are interpolated bilinearly using 4-noded quadrilaterals, and pressure is taken as constant within each element, *e*. Thus, if N_i are the velocity interpolation functions,

$$U^{(e)}(x,y) = \sum_{i=1}^{4} N_i U_i, \tag{14}$$

$$V^{(e)}(x,y) = \sum_{i=1}^{4} N_i V_i, \tag{15}$$

and

$$P^{(e)}(x,y) = P^{(e)} = \text{constant}, \tag{16}$$

where U_i, V_i are the nodal values of *U, V* respectively.

The weight function for the pressure residual is simply unity, so that the pressure residual (corresponding to the continuity Equation (1)) is

$$R_P = \int_{\Omega^{(e)}} \left[\frac{\partial U}{\partial x} + \frac{\partial V}{\partial y} \right] d\Omega^{(e)}, \tag{17}$$

where $\Omega^{(e)}$ is the element area.

Similarly taking N_i as the weight functions, the residuals for the momentum Equations (2-3) are

$$\begin{aligned} R_{U_i} = & \int_{\Omega^{(e)}} N_i \left\{ \left[U\frac{\partial U}{\partial x} + V\frac{\partial U}{\partial y} \right] - \left(\Omega^2 x + 2\Omega V \right) \right\} d\Omega^{(e)} \\ & - \int_{\Omega^{(e)}} N_i \left[\frac{\partial}{\partial x}\left(\frac{2\alpha}{Re}\frac{\partial U}{\partial x} - P \right) + \frac{\partial}{\partial y}\frac{\alpha}{Re}\left(\frac{\partial U}{\partial y} + \frac{\partial V}{\partial x} \right) \right] d\Omega^{(e)}, \end{aligned} \tag{18}$$

and

$$Ri \equiv -2\Omega \frac{\left(\frac{\partial U}{\partial y} - 2\Omega\right)}{\left(\frac{\partial U}{\partial y}\right)} = S(S+1) \tag{4}$$

Depending on whether Ri is greater than or less than zero, local stabilization or destabilization would occur. For turbulent flow, $Ri \cong S$, since $\frac{\partial U}{\partial y}$ is very large near the wall.

Following the conclusions of [1 and 3], Ri is introduced to modify (for rotation) the eddy viscosity expression for stationary pipe or channel flow. The eddy viscosity for flow through stationary channel may be specified *via* a mixing length [13]. However, it is found convenient to use a Van Dreist-type direct expression [15] for the effective kinematic viscosity, υ_e, as

$$\upsilon_e = \frac{\upsilon\left[1+\sqrt{1+4\kappa^2 y^{+2}\left(1-e^{-y^+/26}\right)^2}\right]}{2}, \tag{5}$$

where υ is the laminar kinematic viscosity, $\kappa = 0.4$ is an empirical constant, and y^+ is defined as

$$y^+ = \frac{y u_\tau}{\upsilon}, \tag{6}$$

u_τ being the friction velocity. Equation (6) is used when $0 \le 2\tilde{y}/H \le 0.158$ or when $0.842 \le 2\tilde{y}/H \le 1$, with $\tilde{y} = y + H/2$. When $0.158 < 2\tilde{y}/H < 0.842$, the value of υ_e at $2\tilde{y}/H = 0.158$ is used.

In this study, Equation (5) is modified for rotation introducing Ri. Thus, the viscosity ratio, α is taken as

$$\alpha = \frac{\left[1+\sqrt{1+\frac{4\kappa^2 y^{+2}\left(1-e^{-y^+/26}\right)^2}{(1+\beta Ri)^2}}\right]}{2}, \tag{7}$$

where β is an empirical constant. In this study, it is found that the choice of $\beta = 2$ yields results, which compare well with experiment. For laminar flow, Equations (1-3) are applicable with $\alpha = 1$.

$$R_{V_i} = \int_{\Omega^{(e)}} N_i \left\{ \left[U\frac{\partial V}{\partial x} + V\frac{\partial V}{\partial y} \right] - \left(\Omega^2 y - 2\Omega U \right) \right\} d\Omega^{(e)} - \int_{\Omega^{(e)}} N_i \left[\frac{\partial}{\partial x}\frac{\alpha}{Re}\left(\frac{\partial U}{\partial y} + \frac{\partial V}{\partial x} \right) + \frac{\partial}{\partial y}\left(\frac{2\alpha}{Re}\frac{\partial V}{\partial y} - P \right) \right] d\Omega^{(e)}. \tag{19}$$

In Equations (18-19), the second order derivatives of U and V demand $C^{(1)}$ elements. In order to enable the use of $C^{(0)}$ elements, and simultaneously to invoke any Neumann boundary conditions, the second integrals in Equations (18) and (19) are integrated by parts to yield

$$R_{U_i} = \int_{\Omega^{(e)}} N_i \left\{ \left[U\frac{\partial U}{\partial x} + V\frac{\partial U}{\partial y} \right] - \left(\Omega^2 x + 2\Omega V \right) \right\} d\Omega^{(e)} + \int_{\Omega^{(e)}} \left\{ \frac{\partial N_i}{\partial x}\left(\frac{2\alpha}{Re}\frac{\partial U}{\partial x} - P \right) + \frac{\partial N_i}{\partial y}\frac{\alpha}{Re}\left(\frac{\partial U}{\partial y} + \frac{\partial V}{\partial x} \right) \right\} d\Omega^{(e)} - \int_{\Gamma^{(e)}} N_i \left\{ \left(\frac{2\alpha}{Re}\frac{\partial U}{\partial x} - P \right) n_x + \frac{\alpha}{Re}\left(\frac{\partial U}{\partial y} + \frac{\partial V}{\partial x} \right) n_y \right\} d\Gamma^{(e)}, \tag{18a}$$

and

$$R_{V_i} = \int_{\Omega^{(e)}} N_i \left\{ \left[U\frac{\partial V}{\partial x} + V\frac{\partial V}{\partial y} \right] - \left(\Omega^2 y - 2\Omega U \right) \right\} d\Omega^{(e)} + \int_{\Omega^{(e)}} \left\{ \frac{\partial N_i}{\partial x}\frac{\alpha}{Re}\left(\frac{\partial U}{\partial y} + \frac{\partial V}{\partial x} \right) + \frac{\partial N_i}{\partial y}\left(\frac{2\alpha}{Re}\frac{\partial V}{\partial y} - P \right) \right\} d\Omega^{(e)} - \int_{\Gamma^{(e)}} N_i \left\{ \frac{\alpha}{Re}\left(\frac{\partial U}{\partial y} + \frac{\partial V}{\partial x} \right) n_x + \left(\frac{2\alpha}{Re}\frac{\partial V}{\partial y} - P \right) n_y \right\} d\Gamma^{(e)}, \tag{19a}$$

where $\Gamma^{(e)}$ is the element boundary which coincides with a portion of the domain boundary with specified stress boundary conditions and n_x and n_y are the direction cosines of the outward-directed unit normal to $\Gamma^{(e)}$.

In the present problem, only along the exit, there are Neumann boundary conditions. Along the exit, $n_x = 1$, and $n_y = 0$, the boundary conditions (13c) are applicable. Therefore, the boundary terms in Equation (18a) vanish. In Equation (19a), the surviving boundary term is

$$\int_{\Gamma^{(e)}} N_i \frac{\alpha}{Re} \frac{\partial U}{\partial y} d\Gamma^{(e)} \tag{20}$$

The set of non-linear algebraic equations is solved for the nodal unknowns $\underset{\sim}{U}$, $\underset{\sim}{V}$ and $\underset{\sim}{P}$ using combined Newton's iteration technique. The combined Newton's method requires the derivatives of these residuals with respect to the nodal values of the nodal unknowns U_j, V_j and P_j.

Let

$$\underset{\sim}{X}^{(k)} = \left\{ \underset{\sim}{U}^{T(k)} \;\; \underset{\sim}{V}^{T(k)} \;\; \underset{\sim}{P}^{T(k)} \right\}^T \tag{21}$$

be the vector of the field unknowns at all nodes at k^{th} iteration. The correction vector $\delta \underset{\sim}{X}^{(k)}$ may be obtained as

$$[Q]\left\{ \delta \underset{\sim}{X}^{(k)} \right\} = -\left\{ \underset{\sim}{R}_X^{(k)} \right\}, \tag{22}$$

where

$$[Q] = \begin{bmatrix} \frac{\partial \underset{\sim}{R}_U}{\partial \underset{\sim}{U}} & \frac{\partial \underset{\sim}{R}_U}{\partial \underset{\sim}{V}} & \frac{\partial \underset{\sim}{R}_U}{\partial \underset{\sim}{P}} \\ \frac{\partial \underset{\sim}{R}_V}{\partial \underset{\sim}{U}} & \frac{\partial \underset{\sim}{R}_V}{\partial \underset{\sim}{V}} & \frac{\partial \underset{\sim}{R}_V}{\partial \underset{\sim}{P}} \\ \frac{\partial \underset{\sim}{R}_P}{\partial \underset{\sim}{U}} & \frac{\partial \underset{\sim}{R}_P}{\partial \underset{\sim}{V}} & \frac{\partial \underset{\sim}{R}_P}{\partial \underset{\sim}{P}} \end{bmatrix}, \tag{23}$$

and

$$\underset{\sim}{R}_X = \left\{ \underset{\sim}{R}_U^T \;\; \underset{\sim}{R}_V^T \;\; \underset{\sim}{R}_P^T \right\}^T. \tag{24}$$

The derivatives required in Equation (23) are calculated analytically as

$$\frac{\partial R_P}{\partial U_j} = \int_{\Omega^{(e)}} \frac{\partial N_j}{\partial x} d\Omega^{(e)}, \tag{25a}$$

$$\frac{\partial R_P}{\partial V_j} = \int_{\Omega^{(e)}} \frac{\partial N_j}{\partial y} d\Omega^{(e)}, \tag{25b}$$

$$\frac{\partial R_P}{\partial P_j} = 0, \tag{25c}$$

$$\frac{\partial R_{U_i}}{\partial U_j} = \int_{\Omega^{(e)}} \left[N_i \left(N_j \frac{\partial U}{\partial x} + U \frac{\partial N_j}{\partial x} + V \frac{\partial N_j}{\partial y} \right) + \frac{\alpha}{Re} \left(2 \frac{\partial N_i}{\partial x} \frac{\partial N_j}{\partial x} + \frac{\partial N_i}{\partial y} \frac{\partial N_j}{\partial y} \right) \right] d\Omega^{(e)}, \tag{25d}$$

$$\frac{\partial R_{U_i}}{\partial V_j} = \int_{\Omega^{(e)}} \left[N_i N_j \left(\frac{\partial U}{\partial y} - 2\Omega \right) + \frac{\alpha}{Re} \left(\frac{\partial N_i}{\partial y} \frac{\partial N_j}{\partial x} \right) \right] d\Omega^{(e)}, \tag{25e}$$

$$\frac{\partial R_{U_i}}{\partial P} = -\int_{\Omega^{(e)}} \frac{\partial N_i}{\partial x} d\Omega^{(e)}, \tag{25f}$$

$$\frac{\partial R_{V_i}}{\partial U_j} = \int_{\Omega^{(e)}} \left[N_i N_j \left(\frac{\partial V}{\partial x} + 2\Omega \right) + \frac{\alpha}{Re} \left(\frac{\partial N_i}{\partial x} \frac{\partial N_j}{\partial y} \right) \right] d\Omega^{(e)} - \int_{\Gamma^{(e)}} N_i \frac{\alpha}{Re} \frac{\partial N_j}{\partial y} d\Gamma^{(e)}, \tag{25g}$$

$$\frac{\partial R_{V_i}}{\partial V_j} = \int_{\Omega^{(e)}} \left[N_i \left(N_j \frac{\partial V}{\partial y} + U \frac{\partial N_j}{\partial x} + V \frac{\partial N_j}{\partial y} \right) + \frac{\alpha}{Re} \left(\frac{\partial N_i}{\partial x} \frac{\partial N_j}{\partial x} + 2 \frac{\partial N_i}{\partial y} \frac{\partial N_j}{\partial y} \right) \right] d\Omega^{(e)}, \tag{25h}$$

and

$$\frac{\partial R_{V_i}}{\partial P} = -\int_{\Omega^{(e)}} \frac{\partial N_i}{\partial y} d\Omega^{(e)}. \tag{25i}$$

In these equations, α is treated as a constant in carrying out the differentiation. Hence quadratic convergence property of Newton's method is affected, especially in the initial several iterations.

Once $\underset{\sim}{X}^{(k)}$ is available at k^{th} iteration, then $\underset{\sim}{X}^{(k+1)}$ is obtained as

$$\underset{\sim}{X}^{(k+1)} = \underset{\sim}{X}^{(k)} + \begin{Bmatrix} \alpha_u \delta \underset{\sim}{U}^{(k)} \\ \alpha_v \delta \underset{\sim}{V}^{(k)} \\ \alpha_p \delta \underset{\sim}{P}^{(k)} \end{Bmatrix}, \tag{26}$$

where $\alpha_u, \alpha_v, \alpha_p$ are, respectively, the under-relaxation factors for $\underset{\sim}{U}$, $\underset{\sim}{V}$ and $\underset{\sim}{P}$. The correction vectors $\delta\underset{\sim}{U}^{(k)}$, $\delta\underset{\sim}{V}^{(k)}$ and $\delta\underset{\sim}{P}^{(k)}$ are obtained by solving Equation (22). For convergence, a tolerance of 10^{-5} on the infinity norm of the correction vector is required.

The linear matrix Equation (22) is solved by using a RAM-based frontal solution technique [18]. The advantage of this method is its efficient operation, requiring less computation time than the classical frontal method [19]. All integrals in the element equations are computed using 2×2 Gauss quadrature [17]. Parameter continuation in rotation number is used. Solution at a lower Ro_H is used as the initial guess to obtain the solution at a higher Ro_H.

The computed pressure field is, by choice, discontinuous, and must be smoothed by, for example, a least squares procedure [17] to obtain the nodal pressures from the values of pressure for each element.

RESULTS AND DISCUSSION

Practically identical results were obtained for $Re_H = 11500$, $Ro_H = 0.069$, with 100×16, 150×24 and 200×32 elements, with smooth grading in both directions. A typical quasi-Newton iteration takes 1.4 s for the 100×16, 5.5 s for the 150×24 and 14.5 s for the 200×32 on a 1 GHz Pentium III computer. For all three meshes mass conservation was satisfied to numerical precision. In other words, mass flow rate calculated at any x was practically the same as that at the channel inlet.

Figure 2 shows the effect of mesh refinement on velocity and pressure for $Re_H = 35000$ and $Ro_H = 0.069$. In Figure 2(a), the streamwise velocity, U, along (i) the centerline, (ii) the nodes adjacent to the suction-side wall (SS), and (iii) nodes adjacent to the pressure-side wall (PS) are shown. The maximum difference in velocity between the 100×16 and the 200×32 mesh is about 2%. Similarly, Figure 2(b) shows the pressure distribution for the three meshes. Results are seen to practically coincide for all three meshes. The velocity profiles at $x = 1$ (the expected fully developed position) for the three meshes are also seen in Figure 2(c) to practically coincide. The pressure profiles at $x = 1$ for the three meshes show acceptable level of differences. Thus, due to its computational economy, the 100×16 mesh is used in all subsequent calculations.

In the fully developed region (x ~ 1), the pressure profiles of Figure 2(d) are nearly linear except for a small distance close to the wall. Close to the wall, the streamwise velocity, U decelerates, and hence there is a decrease in the Coriolis acceleration, $2\Omega U$. Right at the wall, due to the no-slip condition, the Coriolis acceleration and hence the pressure gradient, $\frac{\partial P}{\partial y}$, are zero. Thus, the pressure profiles meet the suction- and pressure-side walls at right angles. For turbulent flow, the velocity U quickly reaches the free stream value as the distance from the wall increases, and thereafter, there is no significant change in $2\Omega U$. Thus, the pressure profile is nearly linear (*i.e.*, $\frac{\partial P}{\partial y}$ is constant) for most part of the channel height away from the walls.

Figure 3 shows the velocity vectors and pressure contours computed at $Re_H = 11500$ ($Ro_H = 0.069,\ 0.21$) and $Re_H = 35000$ ($Ro_H = 0.042,\ 0.069$). For easy comparison, dimensional values of velocity (m/s) and pressure (N/m^2) are shown. Naturally, as the Reynolds number increases (compares Figures 3(a) and 3(d)), the U centerline velocity increases. For the same Reynolds number, increasing the rotation number does not result in a significant change in the centerline velocity (although certainly there is asymmetry as seen from the velocity vectors at a given x and as shown in Figure 2(c)). However, as the rotation number increases, at any given x, the pressure increases approximately as the square of the rotation number. The pressure contours slant to the right, again confirming that there is a positive pressure gradient from the suction to the pressure side of the channel.

In addition to the consistency of results from mesh refinement, these physically intuitive results add confidence in the predicted solutions.

Figure 4 shows the variation of friction velocity (at $x = 1$) at the walls as a function of the rotation number for $Re_H = 35000$. Friction velocity is computed using the "law of the wall" modified for rotation (Equation (11)). The friction velocity is normalized with respect to the friction velocity for zero rotation. Thus, at $Ro_H = 0$, the ratio, $u_\tau / u_{\tau 0}$ is unity in Figure 4. The friction velocity on the pressure side reaches an asymptotic value of about 1.17, while on the suction side the friction velocity continues to decrease with increasing rotation number. Similar trends of numerical predictions are also reported by [3-4, 8].

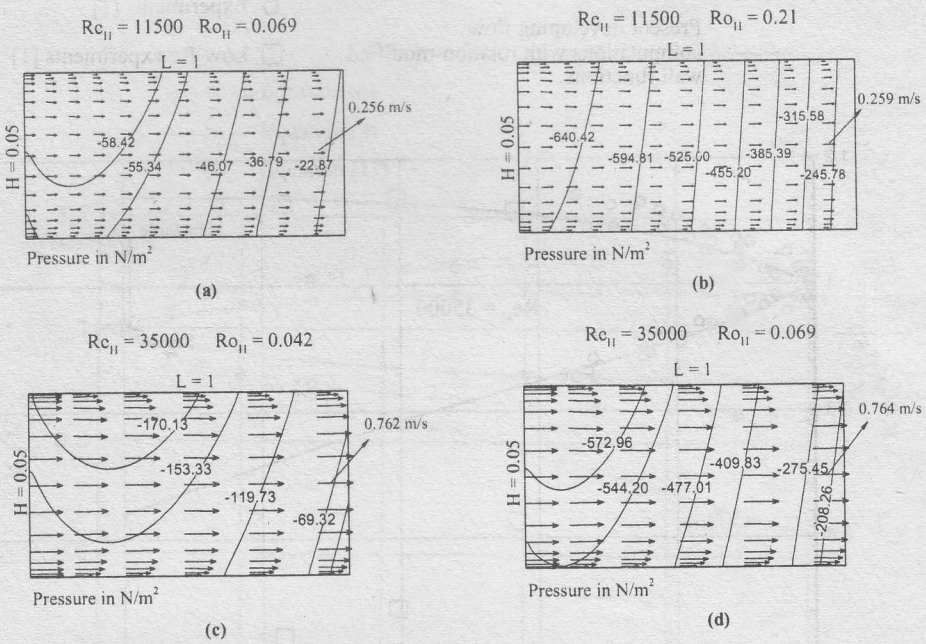

Figure 3. Dimensional velocity vectors and pressure contours for several values of Re_H and Ro_H.

Friction velocity values from the experimental data of [1] are also shown in Figure 4 for comparison. The results agree well for the large Reynolds number experiments. The low-Reynolds number experiments are not expected to agree well, especially on the suction side. Johnston *et. al.* [1] indicate that at low Re_H, there is a tendency for re-laminarization of the boundary layer on the suction side. This cannot be picked up by the present eddy viscosity and wall function model, which are only valid for turbulent flows. On the pressure side, there is no re-laminarization, and hence the present results agree well with experiment.

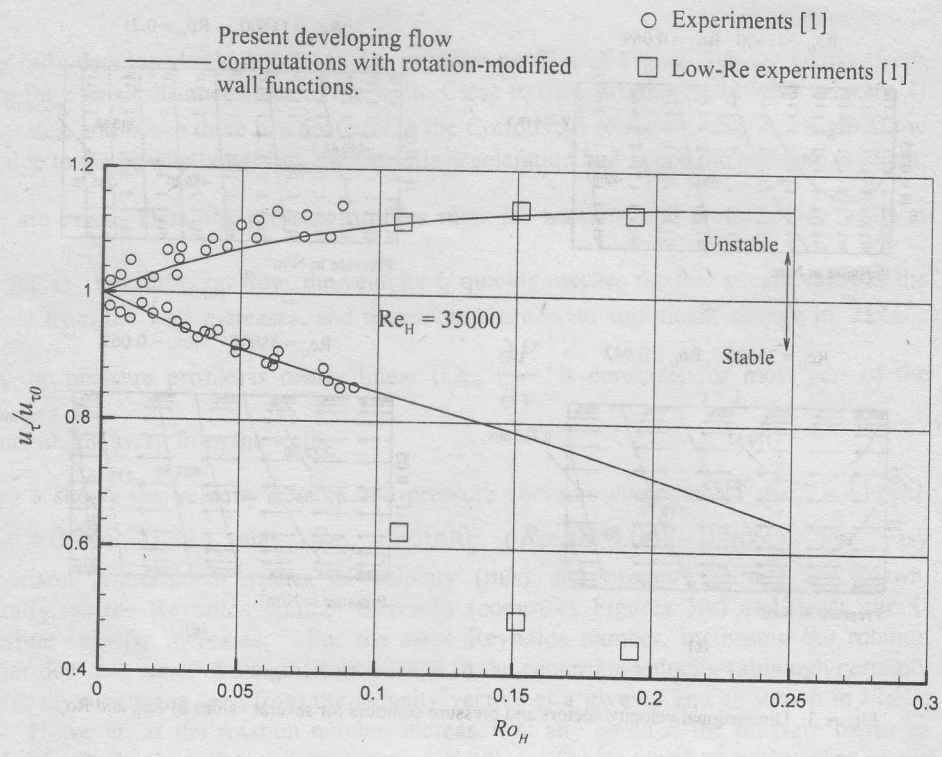

Figure 4. Comparison of computed friction velocity with experiments [1].

Finally, in Figure 5, the friction velocities computed with and without rotation modification (Equations (9) and (11)) are shown. For comparison, results using the linear approximation of Equation (8) are also shown. It is seen that when rotation modification is not used, on the pressure-side, friction velocity reaches a lower asymptotic value of about 1.14, which agrees better with the computed results for fully developed flow [8] using second-moment closure model. However, without modification for rotation, the suction side prediction also reaches an asymptotic value of about 0.8. This is not in good agreement with experimental observations. The use of the linear approximation of Equation (8) predicts an asymptotic behavior of friction velocity on both sides, with lower asymptotic values than when wall functions are used. The conclusion is that much finer grid (near the walls) would be necessary to make the linear approximation viable. In practice, such fine meshes would not only involve significantly large computer time, but they might also introduce difficulties with convergence.

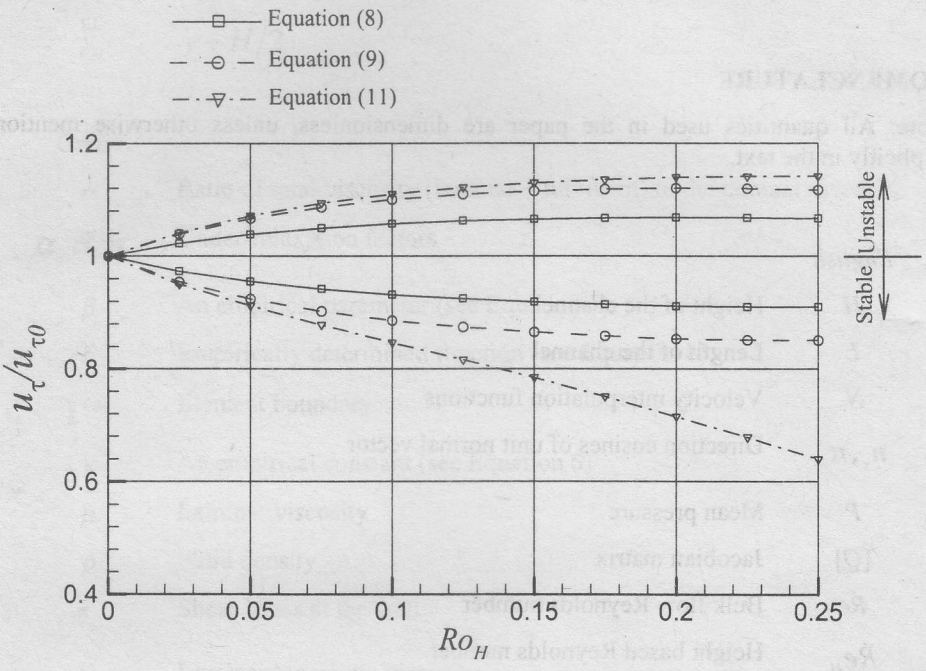

Figure 5. Effect of rotation-modification on wall friction.

CONCLUDING REMARKS

The simple rotation-modified eddy viscosity model, combined with rotation-modified wall functions considered in this study seem to perform well in predicting the developing velocity and pressure fields in rotating channel with sufficient fidelity for engineering purposes. In particular, this conclusion is likely to be useful in computation-intensive problems involving two-phase flow through rotating channels. Experiments indicate that the pressure-side friction velocity approaches an asymptotic value beyond $Ro_H \approx 0.1$, while on the suction side the friction velocity continues to decrease without an asymptotic limit. This trend is well captured by the present simulation. The present study also lends confidence in the efficient use of the hitherto less used finite element methods for this class of problems.

In the present study no-slip boundary conditions are used at the walls of the channel. Wall functions are used to compute the friction velocity, which appears also in the calculation of the eddy viscosity. An interesting and useful extension of this would be to introduce wall functions in specifying boundary conditions as well. This is the subject of a separate paper.

ACKNOWLEDGEMENT

The authors would like to thank Vipin Narang for his help in preparing the manuscript.

NOMENCLATURE

Note: All quantities used in the paper are dimensionless, unless otherwise mentioned explicitly in the text.

English

H	Height of the channel
L	Length of the channel
N_i	Velocity interpolation functions
n_x, n_y	Direction cosines of unit normal vector
P	Mean pressure
$[Q]$	Jacobian matrix
Re	Bulk flow Reynolds number
Re_H	Height based Reynolds number
Ri	Richardson Number
Ro_H	Height based rotation number
Ro_x	Rotation number based on distance x from origin
R_{U_i}, R_{V_i}, R_P	Residuals in Galerkin Weighted Residuals Method with respect to U_i, V_i, P respectively
$\underset{\sim}{R}_X$	Vector defined in Equation (24)
S	A dimensionless parameter (Equation 4)
U	Mean fluid velocity in x-direction
U_0	Inlet mean velocity
u_τ	Friction velocity
V	Mean fluid velocity in y-direction

$\underset{\sim}{X}$	Vector defined in Equation (22)
xyz	Coordinate system attached to rotating reference frame
$\tilde{y}$	$y+H/2$

Greek

α	Ratio of total viscosity (laminar + turbulent) to the laminar viscosity
$\alpha_u\, \alpha_v\, \alpha_p$	Under-relaxation factors
β	An empirical parameter (see Equation 7)
γ	Empirically determined function (see Equation 13)
$\Gamma^{(e)}$	Element boundary
κ	An empirical constant (see Equation 5)
μ	Laminar viscosity
ρ	Fluid density
τ_w	Shear stress at the wall
υ	Laminar kinematic viscosity
υ_e	Effective kinematic viscosity
Ω	Angular velocity
$\Omega^{(e)}$	Element area
$\{\ \}$	Column vector
$\cong$	Approximately equal to
$\equiv$	Is defined as

Subscripts

i, j, k	Dummy indices

Superscripts

+	Non-dimensionalization defined in Equations (6) and (10)
(*e*)	Quantities pertaining to an element
(*k*)	Quantities at the k^{th} Newton's iteration

REFERENCES

[1] Johnston J.P., Halleen R.M. and Lezius D.K., 1972, "Effects of Spanwise Rotation on the Structure of Two-Dimensional Fully Developed Turbulent Channel Flow," *J Fluid Mech.*, Vol. 56, pp. 533-557.

[2] Majumdar A.K., Pratap V.S. and Spalding D.B., 1977, "Numerical Computation of Flow in Rotating Ducts," *ASME Journal of Fluids Engg*, March, pp. 148-153.

[3] Howard J.H.G., Patankar S.V. and Bordynuik R.M., 1980, "Flow Prediction in Rotating Ducts Using Coriolis-Modified Turbulence Models," *ASME J. Fluids Eng*, Vol. 102, pp. 456-461.

[4] Younis B.A., 1993, "Prediction of Turbulent Flows in Rotating Rectangular Ducts," *Transactions of the ASME FED*, Vol. 115, pp. 646-652.

[5] Majumdar A.K. and Spalding D.B., 1977, "Numerical Investigation of Three-Dimensional Flows in a Rotating Duct by a Partially Parabolic Procedure," *ASME Paper* 77-WAFE-7.

[6] Lakshminarayana, B., 1986, "Turbulence Modeling for Complex Shear Flows," *AIAA Journal*, Vol. 24, pp. 1900-1917.

[7] Moore, J., 1967, "Effects of Coriolis on Turbulent Flow in Rotating Channels," *MIT Gas Turbine Lab.* Report 89.

[8] Launder B.E., Tselepidakis D.P. and Younis B.A., 1987, "A Second-Moment Closure Study of Rotating Channel Flow," *J. Fluid Mech.*, Vol. 183, pp. 63-75.

[9] Pagalthivarthi K.V., Desai P.V. and Addie G.R., 1990, "Particulate Motion and Concentration Fields in Centrifugal Slurry Pumps," *Particulate Sci. and Tech.*, Vol. 8, pp. 77-96.

[10] Pagalthivarthi K.V. and Ramanathan V.R., 2001, "Analytical and Numerical Prediction of Inviscid Free Surface Flow in Rotating Channel," *Computers and Fluids* (accepted for publication (MS#00-172)).

[11] Pagalthivarthi K.V., Ramanathan V.R., 2001, "Finite Element Prediction of Viscous Free Surface Flow in Rotating Channel," *Int. J. Num. Meth. Fluids* (accepted for publication (MS#G00-31)).

[12] Hirsch Ch., 1988, "Numerical Computation of Internal and External Flows, Volume 1: Fundamentals of Numerical Discretization," John Wiley and Sons, New York.

[13] White F.M., 1991, "Viscous flow theory," McGraw-Hill, New York.

[14] Bradshaw P., 1969, "The Analogy Between Streamline Curvature and Buoyancy in Turbulent Shear Flow," *J. Fluid Mech.*, Vol. 36, pp. 177-191.

[15] Taylor C., Hughes T.G. and Morgan, K., 1977, "A Numerical Analysis of Turbulent Flow in Pipes," *Computers and Fluids*, Vol. 5, pp. 191-204.

[16] Koyama H., Masuda S., Ariga I. and Watanabe I., 1979, "Stabilizing and Destabilizing Effects of Coriolis Force on Two-Dimensional Laminar and Turbulent Boundary Layers," *ASME J Eng. Power*, Vol. 101, pp. 23-29.

[17] Reddy J.N. and Gartling D.K., 1994, "The Finite Element Method in Heat Transfer and Fluid Dynamics," CRC Press Boca Raton.

[18] Ramanathan V.R., 2000, "Prediction of Two-Phase Free Surface Flow in Rotating Channels," *Doctoral dissertation*, Indian Institute of Technology, New Delhi.

[19] Hood P., 1976, "Frontal Solution Program for Unsymmetric Matrices," *Int J Num Meth Eng.*, Vol. 10, pp. 379-399.